An asymptotic model for elastoplasticity at high stress

P. D. Howell (howell@maths.ox.ac.uk), H. Ockendon
and J. R. Ockendon
Mathematical Institute, 24–29 St Giles', Oxford OX1 3LB, UK

Abstract. This paper describes wave solutions of a model for one-dimensional elastoplasticity under high applied stress in the limit when the plastic wave speed tends to the elastic wave speed. In this parameter regime, a weakly nonlinear asymptotic analysis can be carried out whether or not the plastic flow is rate-dependent. The analysis shows that the plastic waves can catch up with, but not overtake, the elastic waves and also predicts that both compression and expansion shocks can occur when the plastic flow is rate-dependent and the applied stress is sufficiently large.

Keywords: elastoplasticity, rate-dependence, shock waves, weakly nonlinear analysis, singular perturbation

1. Introduction

1.1. Background

This paper describes the systematic asymptotic analysis of the model proposed in [1] for the uniaxial compression of a metal slab. We will only consider the limit of violent compression in which the applied stress greatly exceeds the yield stress, which leads to a considerable simplification in the model. Our principal aim is to elucidate the effect of rate dependence on the simple rate-independent model which results when it is assumed that the yield stress is attained but never exceeded.

In the remainder of this Section, we will restate the dimensionless model derived in [1] and then show how it simplifies in various limits. In Section 2, we will give the boundary and initial conditions appropriate to an impact test and then derive the leading-order asymptotic model that results when the ratio of the yield stress to the applied stress tends to zero. This will involve asymptotic expansions not only in the governing differential equations but also in the shock and other free-boundary conditions that need to be taken into consideration.

We will find that the analysis is relatively straightforward in the rate-independent case, when the leading-order model is a traditional first-order quasilinear hyperbolic partial differental equation that supports elastic and plastic shock waves. In the rate-dependent case, the model becomes a two-dimensional hyperbolic system, numerical solutions of which have been presented in [1]. Guided by these results, we

will present a travelling-wave analysis to show that, whenever the impact is so violent that the plastic compression wave overtakes the elastic shock wave to produce a so-called *over-driven wave*, an associated expansion wave is created in the plastic region.

From an asymptotic viewpoint, the rate-independent model is a singular limit of the rate-dependent model. Although the governing equations form a hyperbolic system in each case, the corresponding characteristics turn out to differ crucially. Consequently, the predictions of the two models disagree both quantitatively and qualitatively for over-driven waves. This represents a fundamental asymptotic nonuniformity which we suggest may arise in many other problems where a singular asymptotic limit reduces a hyperbolic system to another hyperbolic system of lower order.

1.2. The model

In [1], the following dimensionless model has been derived for the axial velocity $v(X,t)$ and stress $\tau(X,t)$ in a slab of metal undergoing violent one-dimensional compression from an impactor. Here X measures Lagrangian distance from the impacted face at $X=0$ and t is time after impact.

(i) *Conservation of mass:*

$$\frac{\partial v}{\partial X} = \frac{\partial}{\partial t}\left(\frac{1}{\rho}\right) = \frac{\partial}{\partial t}\left(F_1 F_2^2\right), \tag{1}$$

where ρ is the density and F_1 and F_2 are the axial and transverse elastic deformation gradients respectively; $F_2 = 1$ when the response is purely elastic and $F_2 < 1$ when it is elastoplastic, in order to compensate for the incompressible plastic deformation.

(ii) *Conservation of Momentum:*

$$\frac{\partial v}{\partial t} = \frac{\partial \tau}{\partial X}. \tag{2}$$

(iii) *Flow rule:*

$$\frac{2}{aF_2}\frac{\partial F_2}{\partial t} = \varepsilon G\left(\frac{\tau - \tau'}{\varepsilon}\right), \tag{3}$$

where a^{-1} is a positive constant that measures the time-scale of the reversion of the stress to the yield surface $|\tau - \tau'| = \varepsilon$, with τ' denoting the transverse stress; $\varepsilon \ll 1$ is effectively the ratio of

the yield stress to the applied stress, and

$$G(z) = \begin{cases} -1+z & z > 1, \\ 0 & |z| \leq 1, \\ 1+z & z < -1. \end{cases}$$

The model is closed by a constitutive law for the elastic deformation and, when this is taken to correspond to mechanical linearity, we obtain the following formulae for the stresses.

(iv) *Constitutive Law:*

$$\tau = \frac{c^2 F_1 + (3-c^2)F_2 - 3}{F_2^2}, \quad \tau' = \frac{(3-c^2)F_1 + (3+c^2)F_2 - 6}{2F_1 F_2}, \tag{4}$$

where c is a positive constant representing the dimensionless elastic wave speed.

The parameter c is related to Poisson's ratio ν by

$$c = \sqrt{\frac{3(1-\nu)}{1+\nu}},$$

and hence lies in the range $\left(1, \sqrt{3}\right)$. An additional lower bound on c was found in [1] to be necessary for physically plausible behaviour to occur as the material yields under compression; in the limit $\varepsilon \to 0$, this reduces to

$$c \gtrsim 1 + \frac{2}{3}\sqrt{\varepsilon}. \tag{5}$$

1.3. Limiting cases and characteristic analysis

In the following section, we will apply the above model to the particular problem of violent impact on a semi-infinite target. Before doing so, here we will briefly list some of the limiting cases in which the system (1–4) reduces to simpler and more familiar models. We will also contrast the characteristics of the hyperbolic systems that result in each case.

(i) *Elastic behaviour*
As long as $|\tau - \tau'| \leq \varepsilon$, the flow rule (3) implies that $F_2 \equiv 1$, assuming that the system was initially unstrained. Hence any purely elastic precursor to plastic flow is described by the linear hyperbolic system $(1, 2, 4)$ with $F_2 = 1$, the characteristics being

$$\frac{\mathrm{d}X}{\mathrm{d}t} = \pm c. \tag{6}$$

(ii) *Extreme plasticity*
A situation where the applied stress greatly exceeds the yield stress is described by taking the limit $\varepsilon \to 0$, so that the right-hand side of (3) is simply $(\tau - \tau')$. Equations (1–4) then comprise another hyperbolic system, now third-order and nonlinear, with characteristics given by

$$\frac{\mathrm{d}X}{\mathrm{d}t} = 0, \quad \pm \frac{c}{F_2^2}. \tag{7}$$

Note that the latter two wave-speeds agree with (6) for elastic waves with $F_2 = 1$.

(iii) *Rate-independent extreme plasticity*
In the rate-independent limit $a \to \infty$ (still also taking $\varepsilon \to 0$), the flow rule (3) simplifes further to the effective yield condition $\tau - \tau' = 0$. Use of (4) then leads to an algebraic relation between F_1 and F_2, and the solution relevant to evolution from an initially unstrained state is simply $F_1 = F_2$. As pointed out in [1], the model thus reduces to the equations of barotropic gasdynamics, with an effective gas law $\tau = 3\left(\rho^{1/3} - \rho^{2/3}\right)$. The characteristics of the resulting two-dimensional hyperbolic system are thus given by

$$\frac{\mathrm{d}X}{\mathrm{d}t} = \pm\sqrt{2\rho^{-1/3} - \rho^{-2/3}} \sim \pm 1 \quad \text{when } \rho \sim 1. \tag{8}$$

This implies that the linear plastic wave speed is unity, whereas the elastic wave speed is c according to (6) (recall that $c > 1$).

(iv) *Linearised extreme plasticity*
The above observations may be reconciled by taking the extreme plasticity limit $\varepsilon \to 0$ and then linearising about the unstressed state with $F_1 = F_2 = 1$ and $v = 0$, to obtain

$$\frac{\partial}{\partial t}\left(\frac{\partial^2}{\partial t^2} - c^2\frac{\partial^2}{\partial X^2}\right)v + \frac{9}{4}a(c^2-1)\left(\frac{\partial^2}{\partial t^2} - \frac{\partial^2}{\partial X^2}\right)v = 0. \tag{9}$$

This reveals that the "plastic" characteristics, given by (8), are subcharacteristics for the third-order hyperbolic system described in (ii) above.

We will now formulate and solve a specific initial/boundary value problem that models impactor tests, as described in [2]. In §2.2 we derive the weakly nonlinear limit model that holds uniformly in time when ε is small and in §2.3 and §2.4 we consider its solution in rate-independent and rate-dependent situations.

2. The impact problem

2.1. Boundary conditions

We consider an initially unstressed target in $X > 0$ with initial conditions

$$v = 0 \quad \text{and} \quad F_1 = F_2 = 1 \qquad \text{at} \quad t = 0,\ X > 0. \tag{10}$$

Since it is more realistic to prescribe the impactor velocity rather than the stress it induces, we impose the boundary condition

$$v = V_0(t) \qquad \text{at} \quad X = 0,\ t > 0, \tag{11}$$

where the impact velocity $V_0(t)$ is assumed to be a known function.

As described in [1], the response to the impact is initiated by an elastic precursor wave which occupies a region of width $O(\varepsilon)$ behind the leading characteristic $X = ct$. In this paper we will be focussing attention on the subsequent elastoplastic wave propagation. Analytical progress in this direction is facilitated by considering a weakly nonlinear regime in which the impact velocity $V_0 = O\left(\varepsilon^{1/2}\right)$ and $c = 1 + O\left(\varepsilon^{1/2}\right)$ which, bearing (5) in mind, is a realistic assumption for hard metals.

2.2. Weakly nonlinear analysis

The distinguished limit in which the effects of geometric nonlinearity and rate dependence are retained is obtained by setting $\alpha = \varepsilon^{1/2}a$ and performing the rescalings

$$c = 1 + \varepsilon^{1/2}\gamma, \quad F_2 = 1 - \varepsilon^{1/2}\phi, \quad \rho = 1 + \varepsilon^{1/2}\varrho, \quad v = \varepsilon^{1/2}\mathfrak{v}, \tag{12}$$

before taking the limit $\varepsilon \to 0$; we note that the condition (5) leads to the restriction

$$\gamma > \frac{2}{3}. \tag{13}$$

The stress components may then be expanded in the form

$$\tau = -\varepsilon^{1/2}\varrho + \varepsilon(\varrho - 3\phi)(\varrho - \phi - 2\gamma) + O\left(\varepsilon^{3/2}\right), \tag{14}$$

$$\tau' = -\varepsilon^{1/2}\varrho + \varepsilon(\varrho - 3\phi)(\gamma - \phi) + O\left(\varepsilon^{3/2}\right), \tag{15}$$

and hence

$$\frac{\tau - \tau'}{\varepsilon} = (\varrho - 3\phi)(\varrho - 3\gamma) + O\left(\varepsilon^{1/2}\right). \tag{16}$$

To lowest order in ε, the governing equations (1–3) therefore become

$$\frac{\partial \varrho}{\partial t} + \frac{\partial \mathfrak{v}}{\partial X} = 0, \qquad \frac{\partial \mathfrak{v}}{\partial t} + \frac{\partial \varrho}{\partial X} = 0, \tag{17}$$

and

$$-\frac{2}{\alpha}\frac{\partial \phi}{\partial t} = G((\varrho - 3\gamma)(\varrho - 3\phi)). \tag{18}$$

The initial and boundary conditions (10,11) give

$$\begin{aligned} \varrho = \mathfrak{v} = \phi = 0 \quad \text{at} \quad t = 0,\ X > 0, \\ \mathfrak{v} = V(t) \quad \text{at} \quad X = 0,\ t > 0, \end{aligned} \tag{19}$$

where $V(t) = \varepsilon^{-1/2} V_0(t)$ is assumed to be monotonic increasing, concave and bounded, so that

$$V(0) = 0,\ V'(t) > 0,\ V''(t) < 0 \text{ and } \lim_{t\to\infty} V(t) = V_{\mathrm{m}}. \tag{20}$$

Hence, when $t > X$, we have

$$\varrho = \mathfrak{v} = V(t - X), \tag{21}$$

whether the material is elastic or plastic. From (18), we deduce that yield first occurs when $\varrho(\varrho - 3\gamma) = -1$ and, as shown in [1], this happens when $t = t_*$, where

$$V(t_*) = V_* = \frac{3}{2}\left(\gamma - \sqrt{\gamma^2 - \frac{4}{9}}\right). \tag{22}$$

The lower bound (13) on γ ensures that V_* is real and lies in the range $(0, 1)$. We assume that the maximum imposed velocity V_{m} exceeds the value V_* so that the material will become plastic when $\mathfrak{v} = V_*$, and ϕ will then be determined by integrating the rate equation (18).

The theory of weakly nonlinear wave propagation [3, 4] tells us that nonlinearity becomes important to lowest order over a long time-scale where $t = O\left(\varepsilon^{-1/2}\right)$. In terms of the travelling-wave variables

$$\eta = X - t, \quad \tau = \varepsilon^{1/2} t, \tag{23}$$

we find that the governing equations (1–3) take the form

$$\frac{\partial \mathfrak{v}}{\partial \eta} - \frac{\partial \varrho}{\partial \eta} + \varepsilon^{1/2}\left(\frac{\partial \varrho}{\partial \tau} + 2\varrho\frac{\partial \varrho}{\partial \eta}\right) = O(\varepsilon), \tag{24}$$

$$\frac{\partial \varrho}{\partial \eta} - \frac{\partial \mathfrak{v}}{\partial \eta} + \varepsilon^{1/2}\left(\frac{\partial \mathfrak{v}}{\partial \tau} + 2\left(2\varrho - 3\phi - 3\gamma\right)\frac{\partial \phi}{\partial \eta} + 2\left(2\phi - \varrho + \gamma\right)\frac{\partial \varrho}{\partial \eta}\right) = O(\varepsilon), \tag{25}$$

$$\frac{2}{\alpha}\frac{\partial \phi}{\partial \eta} - G((\varrho - 3\gamma)(\varrho - 3\phi)) = O\left(\varepsilon^{1/2}\right). \tag{26}$$

By matching with the unstrained material ahead of the travelling wave we obtain the far-field behaviour

$$\varrho,\ \mathfrak{v},\ \phi \to 0 \quad \text{as} \quad \eta \to \infty. \tag{27}$$

We thus deduce from (24) and (25) that

$$\varrho = \mathfrak{v} \tag{28}$$

to lowest order in ε. Then, by adding (24) and (25) to eliminate the dominant term, we obtain the equation

$$\frac{\partial \mathfrak{v}}{\partial \tau} + (2\phi + \gamma)\frac{\partial \mathfrak{v}}{\partial \eta} + (2\mathfrak{v} - 3\phi - 3\gamma)\frac{\partial \phi}{\partial \eta} = 0, \tag{29}$$

while (26) simplifies to

$$\frac{2}{\alpha}\frac{\partial \phi}{\partial \eta} = G((\mathfrak{v} - 3\phi)(\mathfrak{v} - 3\gamma)). \tag{30}$$

Equations (29,30) form a classical hyperbolic system of partial differential equations for the scaled velocity $\mathfrak{v}$ and the plastic strain ϕ, with characteristics given by $\tau =$ constant and $\mathrm{d}\eta/\mathrm{d}\tau = 2\phi + \gamma$. However the rate-independent limit $\alpha \to \infty$ is singular, as we shall see.

Matching with the elastic precursor as $\tau \to 0$ yields the initial condition

$$\mathfrak{v}(\eta, 0) = \begin{cases} V(-\eta) & \eta < 0, \\ 0 & \eta > 0. \end{cases} \tag{31}$$

So long as the material remains elastic, with $\phi = 0$, (29) reduces to

$$\frac{\partial \mathfrak{v}}{\partial \tau} + \gamma\frac{\partial \mathfrak{v}}{\partial \eta} = 0, \tag{32}$$

and the solution is therefore

$$\mathfrak{v} = \begin{cases} V(\gamma\tau - \eta) & -t_* < \eta - \gamma\tau < 0, \\ 0 & \eta - \gamma\tau > 0. \end{cases} \tag{33}$$

This provides the initial condition for the plastic compressive wave solution of (29,30) when $\mathfrak{v} > V_*$, which we consider initially in the rate-independent limit.

2.3. Rate-independent solutions

2.3.1. *Parametric solution*

When $\alpha \to \infty$, (30) reduces to the algebraic equation

$$(\mathfrak{v} - 3\gamma)(\mathfrak{v} - 3\phi) + 1 = 0$$

and hence to

$$\phi = \frac{\mathfrak{v}}{3} - \frac{1}{3(3\gamma - \mathfrak{v})}. \tag{34}$$

This function $\phi(\mathfrak{v})$ is monotonic increasing for $\mathfrak{v} < 3\gamma - 1$ but starts to decrease for larger values of $\mathfrak{v}$. We can expect difficulties as $\mathfrak{v}$ approaches the maximum in ϕ at $\mathfrak{v} = 3\gamma - 1$ so, for the moment, we assume that the maximum imposed velocity lies in the range

$$V_* < V_{\rm m} < 3\gamma - 1. \tag{35}$$

Equation (29) reduces to

$$\frac{\partial \mathfrak{v}}{\partial \tau} + b(\mathfrak{v})\frac{\partial \mathfrak{v}}{\partial \eta} = 0, \quad \text{where} \quad b(\mathfrak{v}) = \mathfrak{v} - \frac{1}{3(3\gamma - \mathfrak{v})^3}, \tag{36}$$

and $b(\mathfrak{v})$ increases monotonically for $\mathfrak{v} \in (V_*, 3\gamma - 1)$. We note that the characteristics $\mathrm{d}\eta/\mathrm{d}\tau = b(\mathfrak{v})$ of (36) are unrelated to either family of characteristics of the full system (29,30), of which they are subcharacterisics (as in the discussion of §1.3).

The solution to (36) satisfying the initial condition (31) may be expressed parametrically as

$$\mathfrak{v} = V(s), \quad \eta = b(V(s))\tau - s, \tag{37}$$

where $s > t_*$ labels the characteristic starting from $\eta = -s$ at $\tau = 0$. In Figure 1, we show the (η, τ)-plane for a typical solution, with, for definiteness, the boundary velocity given by

$$V(t) = V_{\rm m}\left(1 - \mathrm{e}^{-t}\right) \tag{38}$$

and parameter values $V_{\rm m} = 1$ and $\gamma = 1$. Ahead of the leading characteristic $\eta = \gamma\tau$ the material is undisturbed (**U**), with $\mathfrak{v} = \phi = 0$. Between the characteristics $\eta = \gamma\tau - t_*$ and $\eta = \gamma\tau$ (here $t_* \approx 0.48$), the material is elastic (**E**), with $\phi = 0$ and $\mathfrak{v}$ given by (33). The characteristics in the plastic region (**P**) are given by (37), and the leading characteristic is $\eta = b_*\tau - t_*$, where $b_* > \gamma$ is given by equation

$$b_* = b(V_*) = V_* - \frac{V_*^3}{3}. \tag{39}$$

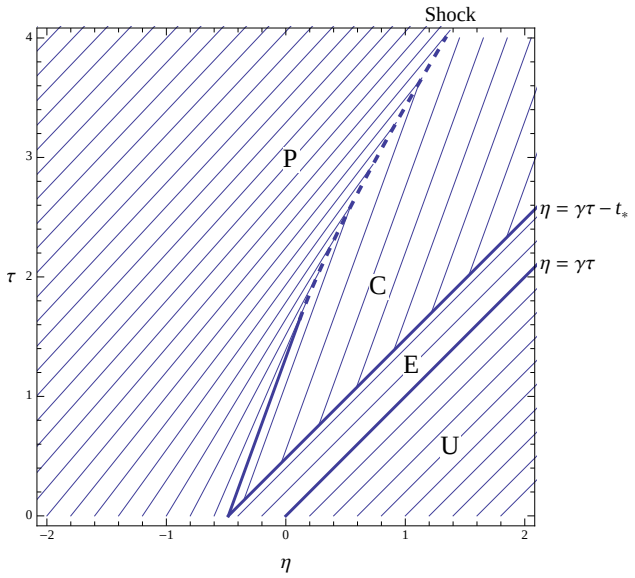

Figure 1. The characteristics in the (η, τ)-plane for the rate-independent weakly nonlinear solution with boundary velocity given by (38) and parameter values $\gamma = 1$, $V_{\rm m} = 1$. The legends **U**, **E**, **C** and **P** indicate the undisturbed, elastic, constant and plastic domains, demarcated by the heavy solid lines, and the heavy dashed curve shows the shock position.

Hence the expanding plastic region lags behind the elastic wave, leaving a constant (**C**) region in between, wherein the material sits on the yield surface with $\phi = 0$ and $\mathfrak{v} = V_*$.

The solution $\mathfrak{v}$ given parametrically by (37) becomes multi-valued for values of s and τ satisfying

$$\tau = \frac{1}{b'(V(s))V'(s)}. \tag{40}$$

With $b(\mathfrak{v})$ given by (36) and $V(t)$ satisfying the conditions (20), the right-hand side of (40) is an increasing function of s, and therefore the shock first forms at $s = t_*$ and

$$\tau = \tau_0 = \frac{1}{b'(V_*)V'(t_*)}, \tag{41}$$

as shown in Figure 1. To continue the solution beyond this time, we must now examine the conservation conditions to be imposed across a shock.

2.3.2. *Asymptotic jump relations*

The Rankine–Hugoniot conditions for equations (1,2) enforcing conservation of mass and momentum across a shock at Lagrangian position $X(t)$ are given by

$$\frac{\mathrm{d}X}{\mathrm{d}t} = -\frac{[v]^+_-}{[1/\rho]^+_-} = -\frac{[\tau]^+_-}{[v]^+_-}. \tag{42}$$

Substituting in the weakly nonlinear expansions (12) and (23), we obtain the approximations

$$1+\varepsilon^{1/2}\frac{\mathrm{d}\eta}{\mathrm{d}\tau} = \frac{[\mathfrak{v}]^+_-}{[\varrho]^+_-}\left\{1+\varepsilon^{1/2}\frac{[\varrho^2]^+_-}{[\varrho]^+_-}+O(\varepsilon)\right\}, \tag{43a}$$

$$1+\varepsilon^{1/2}\frac{\mathrm{d}\eta}{\mathrm{d}\tau} = \frac{[\varrho]^+_-}{[\mathfrak{v}]^+_-}\left\{1-\varepsilon^{1/2}\frac{[(\varrho-3\phi)(\varrho-\phi-2\gamma)]^+_-}{[\varrho]^+_-}+O(\varepsilon)\right\}. \tag{43b}$$

At leading order in ε we clearly have

$$[\varrho]^+_- = [\mathfrak{v}]^+_-, \tag{44}$$

which implies that (28) holds even when shocks are present and we can henceforth set $\varrho \equiv \mathfrak{v}$ everywhere. We can then eliminate the dominant terms by multiplying together (43a) and (43b) to obtain

$$1+2\varepsilon^{1/2}\frac{\mathrm{d}\eta}{\mathrm{d}\tau} = 1+\varepsilon^{1/2}\frac{[\varrho^2-(\varrho-3\phi)(\varrho-\phi-2\gamma)]^+_-}{[\varrho]^+_-}+O(\varepsilon), \tag{45}$$

and hence

$$\frac{\mathrm{d}\eta}{\mathrm{d}\tau} = \frac{[2(2\phi+\gamma)\mathfrak{v}-3(\phi+2\gamma)\phi]^+_-}{2[\mathfrak{v}]^+_-}. \tag{46}$$

Thus conservation of mass and momentum across shocks is enforced in the weakly nonlinear limit by the Rankine–Hugoniot conditions (46) and (44). An entropy condition is normally required to select physically acceptable shock waves, but such a condition is not readily available here, and we will discuss below how causality arguments may instead be used to distinguish physical from unphysical shocks. Figure 1 suggests that we may need to consider more general solutions with jump discontinuities other than shocks in conservation laws and we anticipate three possible categories.

(i) *Elastic/elastic shocks*
For impulsive data with $V(t) \equiv V_{\mathrm{m}}$, a shock separating two elastic regions can occur if $V_{\mathrm{m}} < V_*$. The analysis is greatly simplified by our assumption of mechanical linearity, which means that discontinuities can only travel along the characteristics $\mathrm{d}\eta/\mathrm{d}\tau = \gamma$ of (32).

(ii) *Plastic/plastic shocks*
Next we consider a shock separating two regions in which the material is plastic (as in Figure 1). In the rate-independent limit, we can use (34) to relate ϕ to $\mathfrak{v}$ and hence write (46) in the form

$$\frac{\mathrm{d}\eta}{\mathrm{d}\tau} = \frac{\left[\dfrac{\mathfrak{v}^2}{2} - \dfrac{1}{6(3\gamma - \mathfrak{v})^2}\right]_-^+}{[\mathfrak{v}]_-^+}. \tag{47}$$

This is the Rankine–Hugoniot condition to be applied across a plastic/plastic shock in the weakly-nonlinear regime, and is clearly consistent with the weak solution of the conservation form (36). Now we can apparently select legitimate solutions by ensuring that the characteristics of (36) travel into any shock from either side. However, we will see below that this approach requires care because of the disparity between the characteristics of the rate-independent and rate-dependent models.

(iii) *Elastic/plastic interfaces*
We will also encounter discontinuities at free boundaries separating elastic and plastic regions. The same relations (46) and (44) may be used to ensure conservation of mass and momentum across such a free boundary, but they do not lead to a Rankine–Hugoniot relation like (47) for a traditional one-dimensional conservation law, since the underlying hyperbolic equations are different on either side of the interface. In the elastic material (+, say), we have $\phi = 0$, while in the plastic material (−), ϕ is related to $\mathfrak{v}$ by equation (34), so that (46) becomes

$$\frac{\mathrm{d}\eta}{\mathrm{d}\tau} = \frac{\gamma\mathfrak{v}^+ - \dfrac{1}{3} - \dfrac{(\mathfrak{v}^-)^2}{2} + \dfrac{1}{6\left(3\gamma - \mathfrak{v}^-\right)^2}}{\mathfrak{v}^+ - \mathfrak{v}^-}. \tag{48}$$

We will return to the admissibility of these elastic/plastic discontinuities below.

2.3.3. *Results*

It is convenient to write the shock position $\eta(\tau)$ in the form

$$\eta(\tau) = b(V(\sigma(\tau)))\tau - \sigma(\tau), \tag{49}$$

so that $\sigma(\tau)$ is the value of s labelling the characteristic intersecting the shock from the left at time τ. We substitute this *ansatz* into (47),

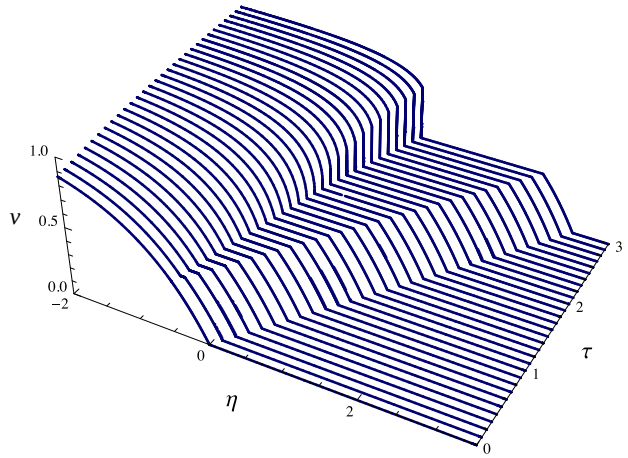

Figure 2. The velocity $\mathfrak{v}$ plotted as a function of η and τ for the rate-independent weakly nonlinear model with boundary velocity given by (38) and parameter values $\gamma = 1$, $V_{\rm m} = 1$.

with $\mathfrak{v}^+ = V_*$ and $\mathfrak{v}^- = V(\sigma(t))$, to obtain the differential equation

$$\left[b'(V(\sigma))V'(\sigma)\tau - 1\right]\frac{\mathrm{d}\sigma}{\mathrm{d}\tau} = (V(\sigma)-V_*)\left\{-\frac{1}{2} + \frac{9\gamma - V(\sigma) - 2V_*}{6(3\gamma - V(\sigma))^3(3\gamma - V_*)^2}\right\}. \quad (50)$$

The initial condition for (50) is found by expanding near $\tau = \tau_0$ to obtain

$$\sigma \sim t_* + \frac{3\,(\tau - \tau_0)}{2}\left\{\frac{-V'(t_*)^2 b'(V_*)^2}{b'(V_*)V''(t_*) + V'(t_*)^2 b''(V_*)}\right\} + O\left((\tau - \tau_0)^2\right). \quad (51)$$

The assumed conditions (20) and (35) ensure that the term in braces is positive and hence that the shock does indeed propagate into the constant region as supposed.

We now return to Figure 1, which shows the results of tracking the shock position using the differential equation (50) and initial condition (51). For $\tau > \tau_0 \approx 1.65$ in this case, a shock forms at the leading edge of the plastic wave and then propagates into the constant region. Since the characteristics travel into the shock from either side, the causality condition is satisfied by this weak solution. The corresponding evolution of the velocity $\mathfrak{v}(\eta, \tau)$ is shown in Figure 2. We see the precursor elastic wave propagating at speed γ followed by a slower nonlinear plastic wave which steepens and eventually forms a shock.

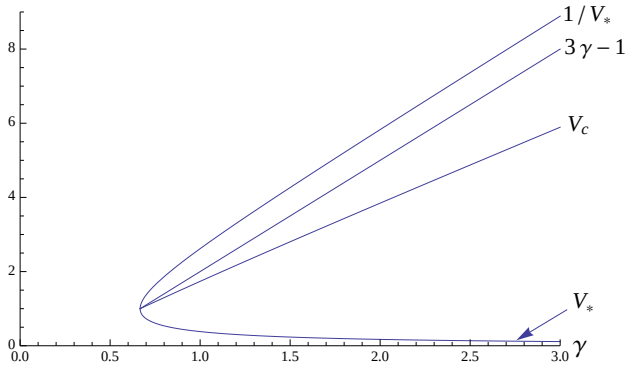

Figure 3. The critical values V_*, V_c and $3\gamma - 1$ of the velocity $\mathfrak{v}$ plotted versus the normalised elastic wave-speed γ. The value $1/V_*$ is shown for future reference.

Equation (50) implies that $\sigma \to \infty$ as $\tau \to \infty$, and the eventual shock velocity is thus given by

$$\frac{\mathrm{d}\eta}{\mathrm{d}\tau} \to \frac{V_\mathrm{m} + V_*}{2} - \frac{6\gamma - V_\mathrm{m} - V_*}{6(3\gamma - V_\mathrm{m})^2(3\gamma - V_*)^2} \quad \text{as } \tau \to \infty. \tag{52}$$

If this velocity exceeds the value γ, then the shock must catch up with the elastic wave, and this occurs if the maximum imposed velocity V_m exceeds the critical value

$$V_\mathrm{c} = \frac{5\gamma}{2} - \sqrt{\frac{1}{3} + \frac{\gamma^2}{4}}. \tag{53}$$

As shown in Figure 3, V_c lies between V_* and $3\gamma - 1$ provided $\gamma > 2/3$. Hence there is a range of values of the velocity $V_\mathrm{m} \in (V_\mathrm{c}, 3\gamma - 1)$ for which the shock will eventually cross the elastic/plastic boundary $\eta = \gamma\tau - t_*$ and turn into an elastic/plastic discontinuity. Subsequently, we will have $\phi^+ = 0$ and $\mathfrak{v}^+$ given by the elastic solution (33) ahead of the shock and ϕ^- given by the yield function (34) behind the shock. The corresponding jump condition (48) may then be written in the form

$$\frac{\mathrm{d}\eta}{\mathrm{d}\tau} = \gamma + \left\{ \frac{(\mathfrak{v}^- - V_*)\,(1/V_* - \mathfrak{v}^-)\,(\mathfrak{v}^- - V_\mathrm{c})\,(5\gamma - V_\mathrm{c} - \mathfrak{v}^-)}{2\,(3\gamma - \mathfrak{v}^-)^2\,(\mathfrak{v}^- - \mathfrak{v}^+)} \right\}, \tag{54}$$

where the term in braces is positive when $\mathfrak{v}^+ < V_* < V_\mathrm{c} < \mathfrak{v}^- < 3\gamma - 1$. Hence the free boundary continues to propagate faster than the elastic wave-speed, thereby crossing the leading characteristic $\eta = \gamma\tau$ and ultimately approaching the speed

$$\lim_{\tau\to\infty} \frac{\mathrm{d}\eta}{\mathrm{d}\tau} = \gamma + \left\{ \frac{(V_\mathrm{m} - V_*)\,(1/V_* - V_\mathrm{m})\,(V_\mathrm{m} - V_\mathrm{c})\,(5\gamma - V_\mathrm{c} - V_\mathrm{m})}{2V_\mathrm{m}\,(3\gamma - V_\mathrm{m})^2} \right\}. \tag{55}$$

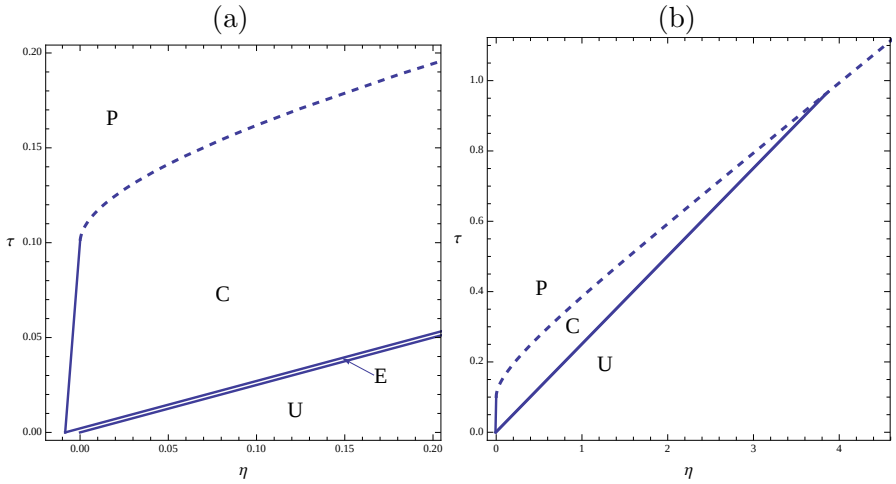

Figure 4. The (η, τ)-plane for the rate-independent weakly nonlinear solution with boundary velocity given by (38) and parameter values $\gamma = 4$, $V_{\rm m} = 10$ shown at two different scales. The dashed curve shows the shock position.

We illustrate this behaviour in Figure 4 for the same boundary velocity function (38) but now using the parameter values $\gamma = 4$ and $V_{\rm m} = 10 > V_{\rm c} \approx 7.92$ in this case. Diagram (a) shows a close-up of the origin in the (η, τ)-plane (for clarity we have omitted the characteristics here and just show the boundaries between the different regions and the shock position). With these parameter values, $t_* \approx 0.0084$ and the elastic region is therefore very narrow. We again see a constant region opening up between the elastic and plastic waves, and a shock that starts at $\tau = \tau_0 \approx 0.1$ before propagating rapidly into the constant region. In diagram (b), we show a longer time-scale over which the shock overtakes the elastic precursor.

The corresponding solution $\mathfrak{v}(\eta, \tau)$ is plotted in Figure 5. Now we see a large-amplitude plastic wave that steepens into a shock and rapidly accelerates, eventually absorbing the relatively feeble elastic precursor. This behaviour is characteristic of experimentally observed over-driven waves [5], in which rapid steepening heralds the plastic wave overtaking the elastic precursor.

As we have already hinted, this scenario can be dramatically changed by the incorporation of rate dependence, as we now describe.

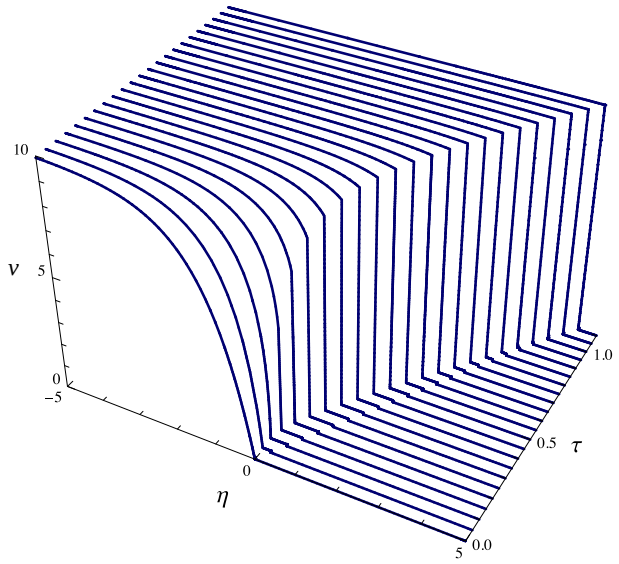

Figure 5. The velocity $\mathfrak{v}$ plotted as a function of η and τ for the rate-independent weakly nonlinear model with boundary velocity given by (38) and parameter values $\gamma = 4$, $V_{\rm m} = 10$.

2.4. Rate-dependent solutions

2.4.1. *"Under-driven" waves*

In order to understand the effects of rate dependence, we first recall some numerical solutions of the system (29,30) which have been given in [1]. When $V_{\rm m} < V_{\rm c}$, so that the plastic wave is not over-driven, the situation is as shown in Figure 6. This suggests that the regularising effect of rate dependence is strong enough that the shock in Figure 2 becomes a smooth wave whose width decreases as the rate constant α increases. We will now verify this analytically by looking for travelling-wave solutions of the rate-dependent model.

2.4.2. *Travelling waves*

We now analyse in detail the travelling-wave solutions discussed in [1]. We seek solutions of the system (29,30) in which $\mathfrak{v}$ and ϕ depend only on the travelling-wave variable $z = \eta - \beta\tau$, where β is the wave-speed (relative to the translating frame (η, τ)). We note in passing that a travelling wave solution in Lagrangian coordinates corresponds also to a travelling wave in the Eulerian frame, albeit one with a different wave-form. We match with the relevant constant solution ahead of the wave and with the imposed maximum velocity behind the wave to obtain

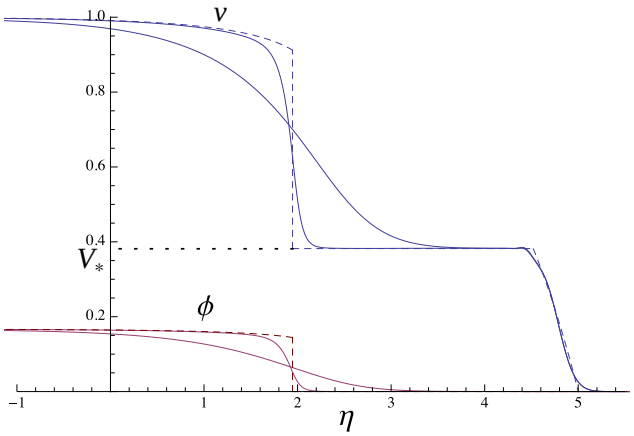

Figure 6. Numerical solutions of the weakly nonlinear rate-dependent model for $\mathfrak{v}$ and ϕ plotted versus η with $\tau = 5$. The parameter values are $\gamma = 1$, $V_{\rm m} = 1$ and $\alpha = 1, 10$. The dashed curve shows the rate-independent limit $\alpha \to \infty$.

the far-field conditions

$$\mathfrak{v} \to V_*, \ \phi \to 0 \quad \text{as} \quad z \to \infty, \tag{56a}$$

$$\mathfrak{v} \to V_{\rm m}, \ \phi \to \phi_{\rm m} \quad \text{as} \quad z \to -\infty, \tag{56b}$$

where

$$\phi_{\rm m} = \frac{V_{\rm m}}{3} - \frac{1}{3\,(3\gamma - V_{\rm m})}. \tag{57}$$

We recall that the right-hand side of (57) is a monotonic increasing function of $V_{\rm m}$ for $V_{\rm m} \in (V_*, 3\gamma - 1)$, and $\phi_{\rm m}$ therefore lies in the range $\phi_{\rm m} \in (0, \gamma - 2/3)$.

Equation (29) becomes

$$(2\phi + \gamma - \beta)\frac{{\rm d}\mathfrak{v}}{{\rm d}z} = (3\phi - 2\mathfrak{v} + 3\gamma)\,\frac{{\rm d}\phi}{{\rm d}z}, \tag{58}$$

which admits the first integral

$$\mathfrak{v} = \frac{2(\gamma - \beta)V_* + 3(\phi + 2\gamma)\phi}{2(2\phi + \gamma - \beta)}, \tag{59}$$

when we impose the matching condition (56a). By substituting this into the other matching condition (56b), we obtain an expression for the wave-speed, namely

$$\beta = \gamma - \frac{(1/V_* - V_{\rm m})\,(V_{\rm c} - V_{\rm m})\,(5\gamma - V_{\rm c} - V_{\rm m})}{2\,(3\gamma - V_{\rm m})^2}. \tag{60}$$

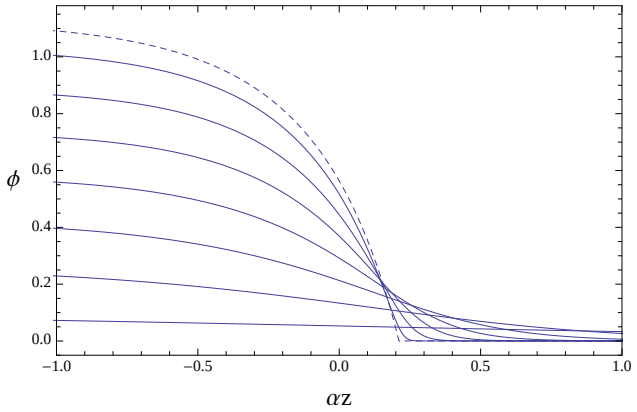

Figure 7. Travelling-wave solution for ϕ plotted versus αz with parameter values $\gamma = 2$ and $V_{\mathrm{m}} = 0.5, 1.0, \ldots, 3.5$. The limiting case $V_{\mathrm{m}} = V_{\mathrm{c}} \approx 3.845$ is shown as a dashed curve.

Note that this reproduces the jump condition (54) derived previously for the rate-independent model, when we put $\mathfrak{v}_- = V_{\mathrm{m}}$ and $\mathfrak{v}_+ = V_*$. We deduce that $\beta < \gamma$, so that the travelling plastic wave propagates more slowly than the elastic wave-speed, provided $V_{\mathrm{m}} < V_{\mathrm{c}}$, again in agreement with the rate-independent results.

Substitution of (59) into (30) leads to an autonomous ordinary differential equation for $\phi(z)$ which may be written in the form

$$\frac{2}{\alpha}\frac{\mathrm{d}\phi}{\mathrm{d}z} = \frac{27\phi\,(\phi-\phi_{\mathrm{m}})}{4\,(2\phi+\gamma-\beta)^2}F(\phi), \tag{61}$$

where

$$F(\phi) = -\phi^2 + A\phi + B, \tag{62a}$$

$$A = \left(\frac{2}{3V_*} + V_*\right) + \frac{\left(3-V_*^2\right)}{9\,(3\gamma - V_{\mathrm{m}})} - \frac{V_*}{9\,(3\gamma-V_{\mathrm{m}})^2} \tag{62b}$$

$$B = \frac{(V_{\mathrm{c}}-V_{\mathrm{m}})\,(5\gamma - V_{\mathrm{c}} - V_{\mathrm{m}})}{(3\gamma - V_{\mathrm{m}})}\left[\frac{1}{3V_*} - \frac{2V_*^2}{9\,(\gamma - V_{\mathrm{m}})} - \frac{V_*}{9\,(3\gamma-V_{\mathrm{m}})^2}\right]. \tag{62c}$$

It is a straightforward exercise to show that $F(0) = B > 0$ and

$$F\left(\gamma - 2/3\right) = \frac{(3\gamma - V_{\mathrm{m}})}{27}\left[\frac{V_*}{(3\gamma-V_{\mathrm{m}})^2} + \frac{V_*\,(1+V_*)}{(3\gamma - V_*)} - 3\right]^2 > 0 \tag{63}$$

for $V_{\mathrm{m}} \in (V_*, V_{\mathrm{c}})$. It follows that $F(\phi) > 0$ for $0 < \phi < \phi_{\mathrm{m}} < \gamma - 2/3$ and hence that the differential equation (61) admits a unique (up to an arbitrary translation) solution satisfying the matching conditions (56).

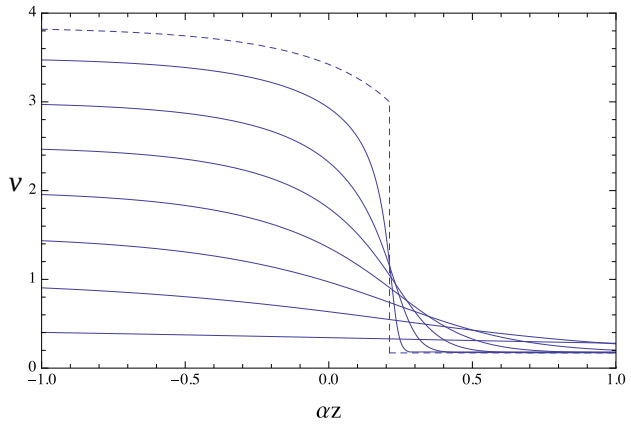

Figure 8. Travelling-wave solution for $\mathfrak{v}$ plotted versus αz with parameter values $\gamma = 2$ and $V_{\rm m} = 0.5, 1.0, \ldots, 3.5$. The limiting case $V_{\rm m} = V_{\rm c} \approx 3.845$ is shown as a dashed curve.

We show typical travelling wave profiles in Figure 7, with $\gamma = 2$ and values of $V_{\rm m}$ varying between $V_* \approx 0.1716$ and $V_{\rm c} \approx 3.845$ in this case. The arbitrary translation of each curve is fixed by choosing $\phi = \phi_{\rm m}/2$ at $z = 0$. In the limit as $V_{\rm m} \searrow V_*$, the wave becomes shallower and wider, with

$$\phi \sim \frac{(V_{\rm m} - V_*)\left(1 - V_*^2\right)}{3\left(1 + {\rm e}^{bz}\right)}, \quad b = \frac{9\alpha\,(V_{\rm m} - V_*)\left(1 + V_*^2\right)}{4\left(1 - V_*^2\right)}. \tag{64}$$

However, at the other extreme where $V_{\rm m} \nearrow V_{\rm c}$, even these rate-dependent solutions develop a slope discontinuity, as shown by the dashed curve in Figure 7, with

$$\phi \to \begin{cases} \dfrac{4V_{\rm c}}{3} - 2\gamma - \dfrac{4(5\gamma - 2V_{\rm c})}{3}\left[\exp\left(-\dfrac{9\alpha}{8}\,(5\gamma - 2V_{\rm c})\,z\right) - 1\right]^{-1} & z < z_{\rm c}, \\ 0 & z > z_{\rm c}, \end{cases} \tag{65}$$

where

$$z_{\rm c} = \frac{8}{9\alpha\,(5\gamma - 2V_{\rm c})} \log\left(\frac{2V_{\rm c} - 3\gamma}{7\gamma - 2V_{\rm c}}\right). \tag{66}$$

The corresponding behaviour of $\mathfrak{v}$ as a function of z is shown in Figure 8. Again we see that the amplitude of the wave increases as $V_{\rm m}$ increases towards its maximum value $V_{\rm c}$. Now the limiting solution is

found from (59) to take the form

$$\mathfrak{v} \to \begin{cases} \dfrac{3}{2}\gamma + \dfrac{3}{4}\phi & z < z_{\rm c}, \\ V_* & z > z_{\rm c}, \end{cases} \tag{67}$$

as $V_{\rm m} \nearrow V_{\rm c}$, with ϕ again given by (65). Hence the solution approaches a shock, across which $\mathfrak{v}$ jumps from V_* to $3\gamma/2$.

To summarise, we have found that the rate-dependent model admits smooth travelling-wave solutions connecting an upstream velocity $V_{\rm m} < V_{\rm c}$ to the velocity V_* in the constant region. The width of these waves scales with $1/\alpha$ so that they are manifested as shocks in the rate-independent limit $\alpha \to \infty$. However, as $V_{\rm m} \nearrow V_{\rm c}$, we observe the formation of a shock that is not regularised by rate-dependent effects, notably one across which ϕ is continuous but $\mathfrak{v}$ is not. For $V_{\rm m} > V_{\rm c}$, we are unable to find any continuous solutions connecting the imposed up- and down-stream conditions. This may appear surprising compared with the rate-independent solution shown in Figures 4 and 5, which suggested that over-driven waves are in fact possible and involve elastoplastic shock waves across which both $\mathfrak{v}$ and ϕ suffer jump discontinuities.

However, we are now in possession of new information from our analysis of rate-dependent travelling waves. From the physical viewpoint, rate-dependence implies that jump discontinuities in ϕ are unacceptable and hence that wave velocities exceeding the elastic wave speed are also unacceptable. Although we can expect smooth solutions of (29,30) to tend to weak solutions of (36) as $\alpha \to \infty$, it is far from clear what happens to discontinuous shock solutions of (29,30) in this limit.

2.4.3. *Over-driven waves*

To gain clues concerning the mathematical structure of evolving over-driven waves, we return to numerical solutions of the rate-dependent model (29,30) obtained in [1]. In Figure 9 we show the evolution of $\mathfrak{v}$ and ϕ with $\alpha = 1$ and $\gamma = 2$, so that $V_* \approx 0.1716$ and $V_{\rm c} \approx 3.845$. We again use the expression (38) for the boundary velocity, here choosing $V_{\rm m} = 4.5 \in (V_{\rm c}, 3\gamma - 1)$.

As expected, the material is undisturbed ahead of the leading characteristic $\eta = \gamma\tau$, behind which a narrow elastic region is followed by an expanding constant region in which $\mathfrak{v} = V_*$ and $\phi = 0$. Behind this we see a plastic wave that steepens to form a shock, across which $\mathfrak{v}$ is discontinuous while ϕ suffers only a jump in its first derivative. Thereafter, the shock propagates at the elastic wave speed γ, and the value of $\mathfrak{v}$ immediately behind the shock increases, ultimately attaining a fixed value. Thus we again have a partially dispersed shock, with

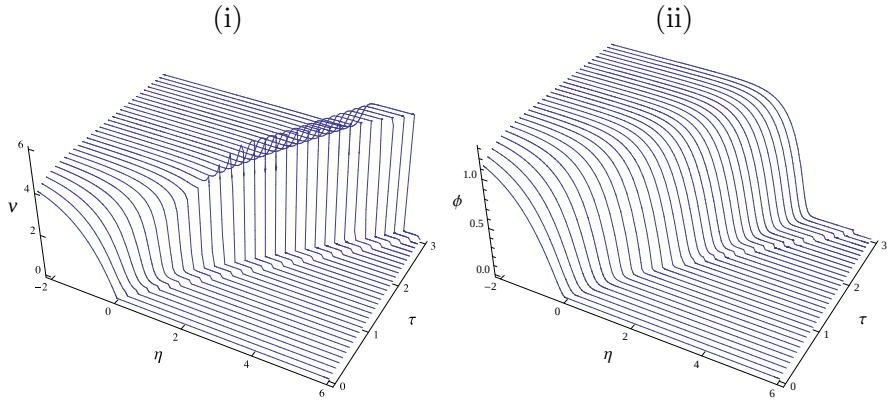

Figure 9. Numerical solution of the weakly nonlinear rate-dependent model in the over-driven regime for (i) $\mathfrak{v}$ and (ii) ϕ plotted versus η with $\tau \in [0, 3]$. The parameter values are $\gamma = 2$, $V_{\rm m} = 4.5$ and $\alpha = 1$.

transition back to the upstream values $\mathfrak{v} = V_{\rm m}$ and $\phi = \phi_{\rm m}$ occurring via a smooth plastic expansion wave that lags behind the discontinuity. Consequently, a plateau opens up between the shock and the following plastic wave, in which $\mathfrak{v}$ takes an approximately constant value significantly in excess of $V_{\rm m}$, while ϕ remains approximately equal to zero.

This numerical experiment immediately suggests that the rate-independent results shown in Figures 4 and 5 cannot be realised as large-α limits of solutions of the evolutionary rate-dependent model. The key new features revealed by Figure 9 are, respectively, the existence of a smooth expansion wave that lags behind the jump discontinuity in $\mathfrak{v}$ and the persistent continuity of ϕ at this elastoplastic shock. This leads us to examine the admissibility of jump discontinuities in $\mathfrak{v}$ from a mathematical viewpoint.

2.4.4. *Rate-dependent shocks and travelling waves*

We have already derived the Rankine–Hugoniot relations (44) and (46) enforcing conservation of mass and momentum across a jump discontinuity. As discussed at the end of §2.4.2, for the rate-dependent model, these must be supplemented by the corresponding relation for the rate equation (30), namely

$$[\phi]^{+}_{-} = 0. \tag{68}$$

We recall that, in §2.3.3, we found solutions of the rate-independent model in which both $\mathfrak{v}$ and ϕ are discontinuous across an elastic/plastic free boundary. The condition (68) confirms that such solutions are indeed impossible for the rate-dependent model.

Applying (68) to the other relations (44) and (46), we find that the shock speed is given by

$$\frac{\mathrm{d}\eta}{\mathrm{d}\tau} = \gamma + 2\phi. \tag{69}$$

As expected, a shock propagating into a region where $\mathfrak{v} = V_*$ and $\phi = 0$ must therefore propagate at the elastic wave-speed γ. Again, this demonstrates that the solutions found in §2.3.3 containing an elastic/plastic free boundary are disallowed when rate dependence is included, since they travel faster than γ.

With the shock speed given by (69) and $\phi = 0$, we can use (29) and (30) to obtain a differential equation for the value of $\mathfrak{v}$ immediately behind an elastoplastic shock, namely

$$\frac{\mathrm{d}\mathfrak{v}}{\mathrm{d}\tau} = \alpha \left(\mathfrak{v} - \frac{3\gamma}{2} \right) (\mathfrak{v} - V_*) \, (1/V_* - \mathfrak{v}) \, . \tag{70}$$

We recall from (67) that, when a smooth plastic travelling wave tends to an elastoplastic shock, the value of $\mathfrak{v}$ immediately behind the shock is given by $\mathfrak{v} = 3\gamma/2$. As soon as $\mathfrak{v}$ exceeds this value, equation (70) indicates that it will increase towards the next stable equilibrium of (70), namely $\mathfrak{v} = 1/V_*$. We also recall from the discussion before (35) that, since $1/V_* > 3\gamma - 1$, the analysis of solutions of (29) becomes more difficult behind the shock. However, the prediction from (70) exactly matches the behaviour observed in Figure 9(i): once a shock has formed, the value of $\mathfrak{v}$ behind the shock increases rapidly from $3\gamma/2$ ($= 3$ in the case of Figure 9) to $1/V_*$ (≈ 5.828). To understand fully the birth and evolution of the over-driven elastoplastic shock, we need to reconsider the layout of the characteristics.

For reference, in Figure 10(i), we plot the characteristics $\mathrm{d}\eta/\mathrm{d}\tau = b(\mathfrak{v})$ of (36) in the case $\gamma = 4$, $V_\mathrm{m} = 10$ which corresponds to the solution shown in Figure 5. (Figure 10(i) differs from Figure 4 only in that the elastic region is invisible on this scale.) We now contrast this figure with that in Figure 10(ii), which displays the family of characteristics $\mathrm{d}\eta/\mathrm{d}\tau = 2\phi + \gamma$ of the full rate-dependent model (29,30). This reveals that, as soon as there is any rate dependence, the associated *super*characteristics of (30) become tangent to the elastoplastic shock when its speed reaches the value γ, at $(\eta, \tau) = (\eta_\mathrm{s}, \tau_\mathrm{s})$, say.

For smaller values of η and τ, the solutions corresponding to Figures 10(i) and (ii) are identical. However, were the (rate-dependent) compressive wave allowed to accelerate beyond the speed γ as in Figures 4 and 10(i), causality would be violated, since Figure 10(ii) shows that there would be no outgoing supercharacteristics at the shock (a similar configuration of characteristics and shocks has been discussed in [6]).

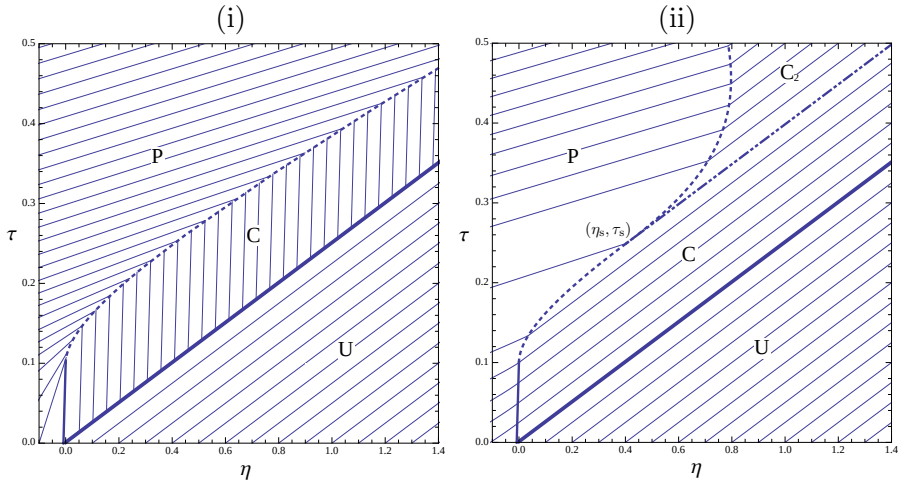

Figure 10. The (η, τ)-plane for the rate-independent solution with boundary velocity given by (38) and parameter values $\gamma = 4$, $V_m = 10$. The heavy solid curves delineate the undisturbed (**U**), constant (**C**, $\mathbf{C_2}$) and plastic (**P**) regions. (i) The heavy dashed curve indicates the shock position and the lighter curves show the characteristics of the rate-independent equation (36). (ii) The heavy dashed curve indicates the dispersed shock position; the dot-dashed curve shows the non-dispersed shock position; the lighter curves show the characteristics of the rate-dependent equation (29).

Beyond the point (η_s, τ_s), the only configuration for a weak solution of (29,30) that satisfies causality is for the compressive shock to continue at speed γ and for an expansion wave to be born at (η_s, τ_s) which lags behind the leading shock. As indicated in Figure 10(ii), the expansion wave and the compressive shock are separated by the expected new constant region $\mathbf{C_2}$ in which $\mathfrak{v} = 1/V_*$ and $\phi = 0$.

To describe the situation quantitatively, we note that the speed of the expansion wave is given by the plastic/plastic Rankine–Hugoniot condition (47), with $\mathfrak{v}_+ = 1/V_*$, which may be rearranged to

$$\frac{\mathrm{d}\eta}{\mathrm{d}\tau} = \gamma - \frac{(\mathfrak{v}_- - V_*)\,(\mathfrak{v}_- - V_c)\,(5\gamma - V_c - \mathfrak{v}_-)}{2\,(3\gamma - \mathfrak{v}_-)^2}, \tag{71}$$

with $\mathfrak{v}_-$ given by the parametric solution (37); the characteristics and shocks shown in Figure 10 for $\eta > \eta_s$ were computed on the basis of the scenario outlined above and (71).

2.4.5. *Over-driven travelling waves*

The computations shown in Figure 9 reveal that the expansion shock is fully dispersed by rate-dependence. Its local structure is therefore described by a rate-dependent travelling wave which may be analysed as in §2.4.2; the only modification required is to replace the matching

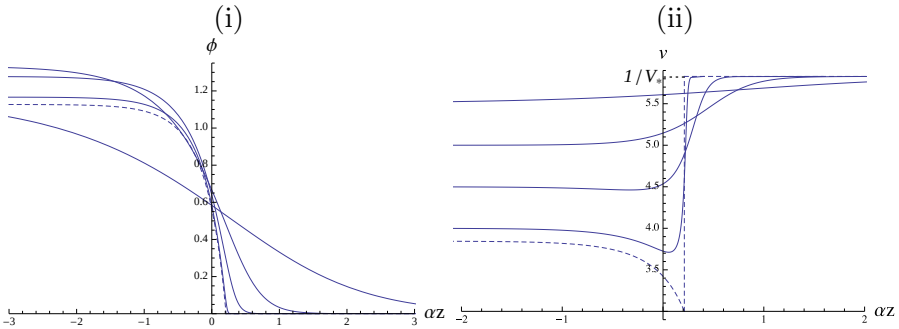

Figure 11. Over-driven travelling-wave solutions for ϕ and $\mathfrak{v}$ plotted versus αz for parameter values $\gamma = 2$ and $V_\mathrm{m} = 4.0, 4.5, 5.0, 5.5$. The limiting case $V_\mathrm{m} = V_\mathrm{c} \approx 3.845$ is shown as a dashed curve.

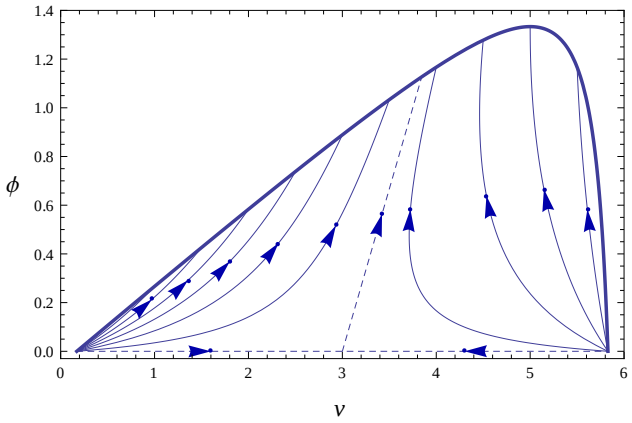

Figure 12. Travelling-wave solutions plotted in the $(\mathfrak{v}, \phi)$-plane for parameter values $\gamma = 2$ and $V_\mathrm{m} = 1.5, 2.0, \ldots, 5.5$. The limiting case $V_\mathrm{m} = V_\mathrm{c} \approx 3.845$ is shown as a dashed curve.

condition (56a) with

$$\mathfrak{v} \to 1/V_*, \ \phi \to 0 \quad \text{as} \quad z \to \infty. \tag{72}$$

The resulting profiles for ϕ and w are plotted in Figure 11 with $\gamma = 2$ and different values of $V_\mathrm{m} > V_\mathrm{c} \approx 3.845$. The dashed curves showing the limiting case as $V_\mathrm{m} \searrow V_\mathrm{c}$ are identical to those shown in Figures 7 and 8, with a slope discontinuity in ϕ and a jump discontinuity in $\mathfrak{v}$, and the amplitudes of the waves decrease as V_m increases from V_c.

We find that smooth connections between V_m and $1/V_*$ exist for all $V_\mathrm{m} \in (V_\mathrm{c}, 1/V_*)$, and they are summarised in Figure 12 along with those found in §2.4.2 for $V_\mathrm{m} \in (V_*, V_\mathrm{c})$. Here we plot the travelling waves as trajectories in the $(\mathfrak{v}, \phi)$-plane; the heavy curve is (34) and the arrows indicate the direction of increasing time for a material particle, corresponding to the direction of *decreasing* z. Each wave is required to

start and end on the yield surface, with $\phi \to 0$ as $t \to -\infty$ and $\mathfrak{v} \to V_{\rm m}$ as $t \to +\infty$. For $V_* < V_{\rm m} < V_{\rm c}$, the corresponding trajectory starts from $(V_*, 0)$, while for $V_{\rm c} < V_{\rm m} < 1/V_*$, the material undergoes a shock from $(V_*, 0)$ to $(1/V_*, 0)$, which then connects smoothly to $(V_{\rm m}, \phi_{\rm m})$. In the limiting case $V_{\rm m} = V_{\rm c}$, either starting point is possible and results in a discontinuous solution represented by two dashed straight lines in the $(\mathfrak{v}, \phi)$-plane.

3. Conclusions

In this paper we have used asymptotic analysis to study a model of one-dimensional elastoplastic wave propagation derived previously in [1]. First taking the "extreme plastic" limit $\varepsilon \ll 1$, in which the applied stress greatly exceeds the yield stress, we used a weakly nonlinear wave analysis to derive a new leading-order model combining the effects of elastic and plastic deformation, mechanical nonlinearity and rate dependence.

Our subsequent focus is on understanding the behaviour of the system in the "rate-independent" limit $\alpha \to \infty$, when the material is constrained to lie on the yield surface when deforming plastically. With $\alpha = \infty$, the governing equations (29,30) reduce from a two-dimensional hyperbolic system to a single quasilinear hyperbolic partial differential equation (36). The limit $\alpha \to \infty$ is therefore singular, and it is to be expected that the rate-dependent model admits smooth solutions which steepen into shocks as the rate parameter α tends to infinity, as in Figure 6. We find that the propagation speed of these dispersed shocks increases with the imposed impact velocity $V_{\rm m}$, reaching the elastic wave-speed at a critical value $V_{\rm m} = V_{\rm c}$.

For "over-driven" waves, where $V_{\rm m} > V_{\rm c}$, the behaviour changes dramatically. The rate-independent model allows a plastic shock wave to accelerate beyond the elastic wave-speed, eventually overtaking the elastic precursor and turning into an elastic/plastic free boundary across which the velocity $\mathfrak{v}$ and plastic strain ϕ are both discontinuous, as in Figure 5. In contrast, rate-dependent over-driven waves cannot exceed the elastic wave-speed and do not admit discontinuities in ϕ. They manage to satisfy the required conservation conditions by instead producing a plastic expansion wave which propagates backwards relative to the advancing shock, as in Figure 9. We were able to explain the details of this behaviour in terms of "plateau" regions, in which the dependent variables are constant to leading order, separated by local shocks and smooth travelling waves, as summarised in Figure 12.

As pointed out in §2.3.2, there is no obvious entropy condition to supplement the derived jump conditions enforcing conservation of mass and momentum, so we must resort to causality arguments to identify physically acceptable shock waves. Over-driven shocks such as that shown in Figure 5 satisfy causality with respect to the characteristics of the rate-independent equation (36), but not with respect to the "supercharacteristics", *i.e.* the characteristics of the underlying rate-dependent model. This explains why the rate-dependent and rate-independent solutions do not converge as the rate parameter α tends to infinity.

Our simple model therefore illustrates a fascinating manifestation of asymptotic nonuniformity. By eliminating the η-derivative in equation (30), taking the limit $\alpha \to \infty$ not only reduces the order of the system but also completely changes the characteristics of the resulting hyperbolic problem (this is true also for the full model (1–4), as shown in §1.3). This does not matter provided the underlying rate-dependent solution remains smooth, but when the rate-dependent solution develops a shock, the behaviour depends profoundly on which characteristics are used to determine its causality.

Acknowledgements

We are grateful to AWE for initiating our interest in this class of problems and especially to Dr Chris Robinson and Dr John Curtis for many useful discussions. We are also indebted to Prof. Dennis Grady and Prof. Justin Wark for their helpful advice. JRO acknowledges receipt of a Leverhulme Emeritus Fellowship during the preparation of this paper.

The authors would like to acknowledge Milton Van Dyke's inspirational contributions to applied mathematics and especially to asymptotic analysis. The senior authors in particular fondly remember his friendliness, charm and patience over a period of 40 years.

References

1. Howell PD, Ockendon H, Ockendon JR (2012) Mathematical modelling of elastoplasticity at high stress. Proc Roy Soc A (submitted)
2. Davison L (2010) Fundamentals of shock wave propagation in solids. Springer-Verlag, Berlin Heidelberg
3. Whitham GB (1974) Linear and nonlinear waves. Wiley, New York
4. Kevorkian JK, Cole JD (1996) Multiple scale and singular perturbation methods. Springer-Verlag, New York

5. Kalantar DH, Belak JF, Collins GW, Colvin JD, Davies HM, Eggert JH, Germann TC, Hawreliak J, Holian BL, Kadau K, Lomdahl PS, Lorenzana HE, Meyers MA, Rosolankova K, Schneider MS, Sheppard J, Stölken JS, Wark JS (2005) Direct observation of the α-ϵ transition in shock-compressed iron via nanosecond X-ray diffraction. Phys Rev Lett 95:075502
6. Lee-Bapty IP, Crighton DG (1987) Nonlinear wave motion governed by the modified Burgers equation. Phil Trans Roy Soc Lond A 323:173–209